Correction of the impact of the absorption of atmospheric gases

Algorithm Theoretical Basis Document

Jürgen Fischer, Rene Preusker, Rasmus Lindstrot

Free University Berlin

Title: **Correction of the impact of the absorption of atmospheric gases**

Document Number: **S3-L2-SD-03-C03-FUB-ATBD_GaseousCorrection**

Issue: **2.2**

Date: **04/08/2010**

	Name	**Function**	**Company**	**Signature**	**Date**
Prepared	Jürgen Fischer	Consultant	FUB		04/08/2010
Approved	O. Fanton d’Andon	OLCI Coordinator	ACRI-ST		
Released	S. Lavender	Project Manager	ARGANS Ltd	SJLavender	Digitally signed by Samantha Lavender DN: cn=Samantha Lavender, o=ARGANS Ltd, ou=Managing Director, email=samantha.lavender@argans.co.uk, c=GB Date: 2010.08.04 13:27:31 +01'00'

Change record

Issue	Date	Description	Change pages
1.0	21/08/2009	Version 1 (PDR delivery)	
2.0	08/04/2010	CDR delivery	
2.1	03/05/2010	Minor updates with Track Changes	
2.2	08/07/2010	Final review / updates before delta CDR release	Table 1 added; increased content within Section 3.2
2.2	04/08/2010	Minor change – so, no change of version	Table 1 corrected

Distribution List

Organisation	To
ESA	Philippe Goryl, Alessandra Buongiorno and Carla Santella
EUMETSAT	Vincent Fournier-Sicre and Vincenzo Santacesaria
CONSORTIUM PARTNERS	ARGANS, ACRI-ST, RAL, Brockmann Consult, Elsag-Datamat

Table of Contents

List of Figures

1. INTRODUCTION

1.1 Acronyms and Abbreviations

AERONET	Aerosol Robotic Network
ARM US	Atmospheric Radiation Measurement program
ATBD	Algorithm theoretical basis document
AATSR	Advanced Along Track Scanning Radiometer (ESA)
BRDF	Bi-directional reflectance distribution function
BSRN	Baseline surface radiation network
CDR	Critical Design Review
CO2	Carbon dioxide
DUE	Data User Element of the ESA Earth Observation Envelope Programme
ECSS	European Cooperation for Space Standardization
EO	Earth observation
ENVISAT	Environmental Satellite, ESA
HITRAN	High-resolution transmission molecular absorption database
H2O	water vapour
MERIS	Medium resolution imaging spectrometer (ESA)
MODIS	Moderate resolution imaging spectroradiometer (NASA)
NetCDF	Network Common Data Format
NOAA	National Oceanic and Atmospheric Administration
NO2	Nitrogen dioxide
NWP	Numerical weather prediction
OLCI	Ocean and land colour instrument
O2	Oxygen
PDF	Probability density function
PDR	Preliminary Design Review
QA	Quality assessment
QR	Qualification Review
RB	Requirements Baseline document
RD	Reference document
SLSTR	Sea and land surface temperature radiometer
TOA	Top of atmosphere

1.2 Purpose and Scope

This ATBD describes the impact of the relevant absorption features due to atmospheric gases within the spectral domain of OLCI. Procedures will be discussed to correct the influence of atmospheric gas absorption for those OLCI channels, which are significantly affected.

1.3 Algorithm Identification

OLCI_trans_corr

2. ALGORITHM OVERVIEW

The radiative transfer processes in the atmosphere and thus OLCI measurements are mainly affected by:

1. air - molecular scattering
2. ozone – absorption
3. water vapour - absorption
4. oxygen – absorption
5. nitrogen-dioxide absorption
6. chlorine dioxide - absorption
7. aerosols - scattering and absorption
8. clouds - scattering and absorption.

All the atmospheric constituents have to be investigated to estimate the impact of atmospheric gases on OLCI measurements in general. The amount of absorption as well as the vertical distribution of each atmospheric gas determines the impact and the strategy for the correction of its impact. Table 1 lists all OLCI channels and the atmospheric gases of a potential impact.

This ATBD describes the impact of the atmospheric gases on the OLCI channels and the method for correcting these impacts.

2.1 Objectives

The absorption of atmospheric gases affects the measured radiances at the OLCI channels depending on the spectral position and width. Since the features of the atmospheric gases are spectrally pronounced, the spectral position of each individual channel, modified by the smile effect (Delwart et al., 2007; Bourg, 2010) might be corrected to a different amount.

For this investigation a mid-latitude summer atmosphere with a total water vapour content of 2.9 g/cm^2 is assumed, whereby the transmission is estimated for an air-mass of 3 to account for the observation geometries. An ozone concentration equivalent to 0.336 cm, a nitrogen dioxide load of 6.86+10^{15} mol/cm^2 are assumed. The carbon dioxide is considered to be 380ppm.

The atmospheric transmission of a mid-latitude summer atmosphere and an air-mass of three within the spectral domain of OLCI are shown in Figure 1. The most dominating gas is water vapour and has to be corrected carefully, considering that water vapour varies in time and space significantly. Ozone effects the radiation mainly in the range between 500 and 700 nm and has to be corrected with respect to the actual ozone concentration. Carbon dioxide has only a weak absorption lines around 1040 nm

Channel	Central wavelength [nm]	Width [nm]	Atmos. gases
O 1	400	15	NO2
O 2	412.5	10	NO2
O 3	442.5	10	NO2, H2O, O3
O 4	490	10	O3
O 5	510	10	H2O, O3
O 6	560	10	O3
O 7	620	10	O3
O 8	665	10	H2O, O3
O 9	673.75	7.5	O3
O 10	681.25	7.5	H2O, O3
O 11	708.75	10	H2O, O3
O 12	754.75	7.5	O3
O 13	761.25	2.5	O2, O3
O 14	764.375	3.75	O2, O3
O 15	767.5	2.5	O2, O3
O 16	778.75	15	O2, O3, H2O
O 17	865	20	H2O
O 18	885	10	H2O
O 19	900	10	H2O
O 20	940	20	H2O
O 21	1020	40	H2O

Table 1: Number, central wavelength and spectral width of all OLCI channels.

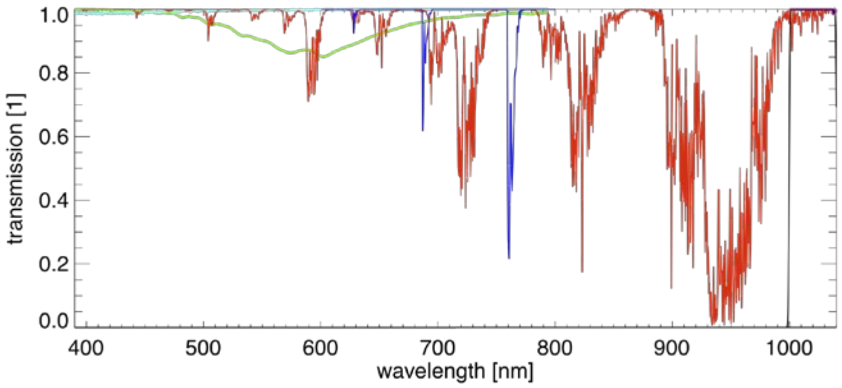

Figure 1: Transmission due to water vapour (red), nitrogen dioxide (bluish), and ozone (green).

Channel 400 nm – atmospheric correction

The new defined OLCI channel at 400nm is influenced by nitrogen dioxide and to a minor extent by water vapour (Figure 2). There is also a very weak absorption by chlorine dioxide, which is not visible in the figure. When no correction will be applied, an inaccuracy of even more than 1% has to be taken into account. Water vapour contributes to variations in the signals by 0.12% between dry and a mid-latitude summer atmosphere (McClatchey et al, 1972; see table 2).

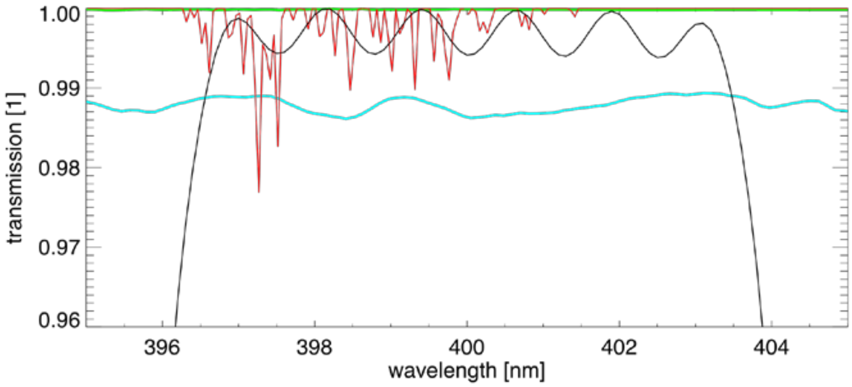

Figure 2: Transmission due to water vapour (red), nitrogen dioxide (bluish), ozone (green), and OLCI filter function in black within the spectral domain of channel@400nm.

Channel 412.5 nm – chlorophyll absorption

This channel is affected by nitrogen dioxide. The impact on the radiances is in the same order of that in the 400nm channel (see table 2). Since nitrogen dioxide is variable in the atmosphere and is not be monitored on a regular basis, a certain inaccuracy might be remain.

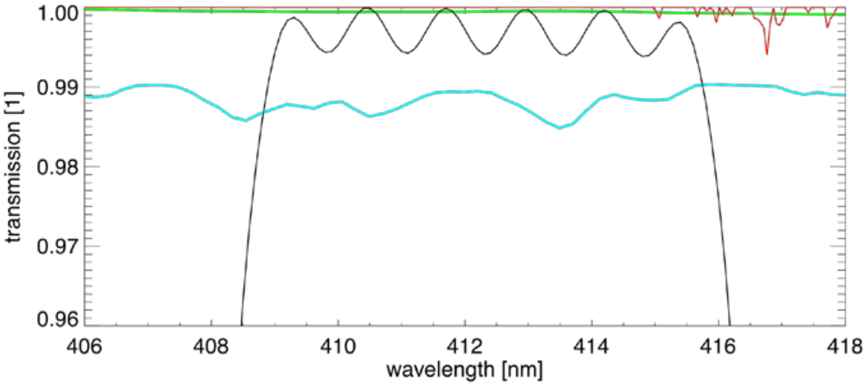

Figure 3: Transmission within channel@412.5nm, see figure 2.

Channel 442.5 nm

Channel 442.5nm is affected by nitrogen dioxide and by ozone to a minor extent; however, both atmospheric gases can contribute to a reduction of the measured radiances by 1.5% (figure 4). Water vapour has some stronger absorption lines, leading to total change of 0.8% in the signal when the atmosphere change from dry to a mid-latitude summer (table 2). An adequate correction of the affect due to the absorption of these gases is required to achieve sufficient accuracy.

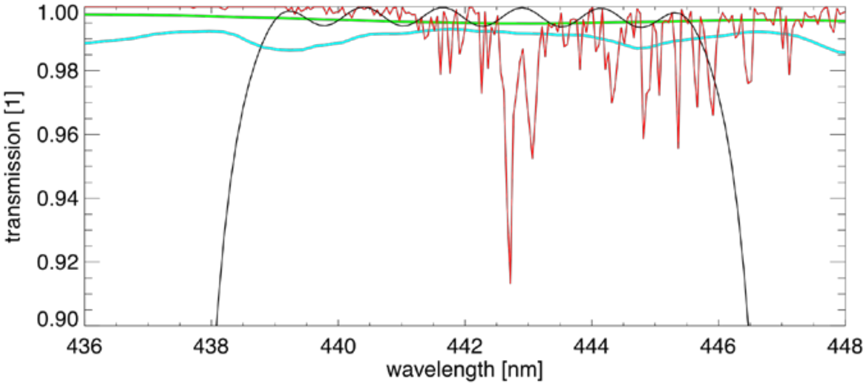

Figure 4: Transmission within channel@442.5nm, see figure 2.

Channel 490 nm

Channel 490nm is affected by ozone and nitrogen dioxide leading to a reduction of the measured radiances by 2.5% and 0.5%, respectively (figure 5 and table 2). Water vapour can contribute by roughly 0.2%. A correction of the impact of the absorption of ozone is necessary and of nitrogen dioxide is eligible to avoid misinterpretation of the OLCI measurements.

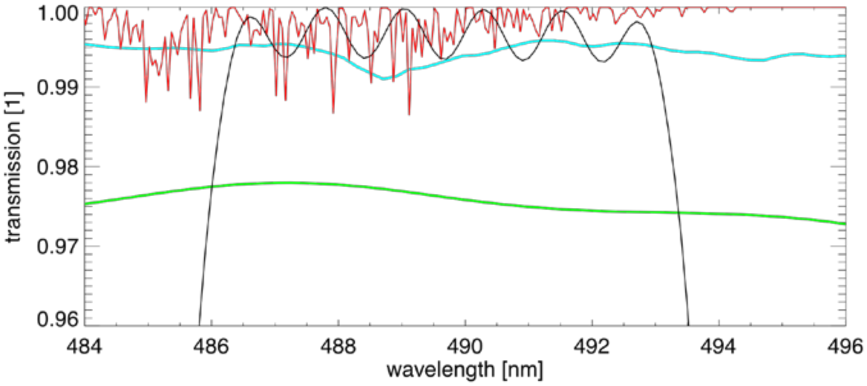

Figure 5: Transmission within channel@490nm, see figure 2.

Channel 510 nm - pigment concentration

This channel is affected quite strongly by ozone (figure 6). Water vapour and nitrogen dioxide can additionally reduce the signal by 2% and 0.5% (table 2). A correction of the impact of the absorption of at least ozone and water vapour has to be performed.

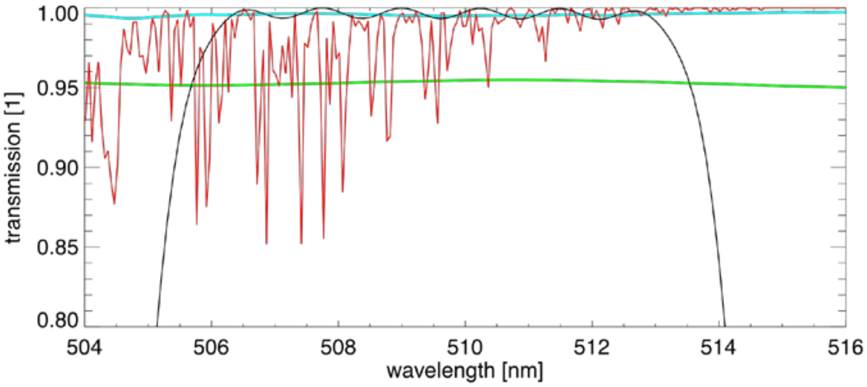

Figure 6: Transmission within channel@510nm, see figure 2

Channel 560 nm – pigment concentration

This channel is affected quite strongly by ozone (figure 7). A correction of the impact of the absorption of ozone is inevitable.

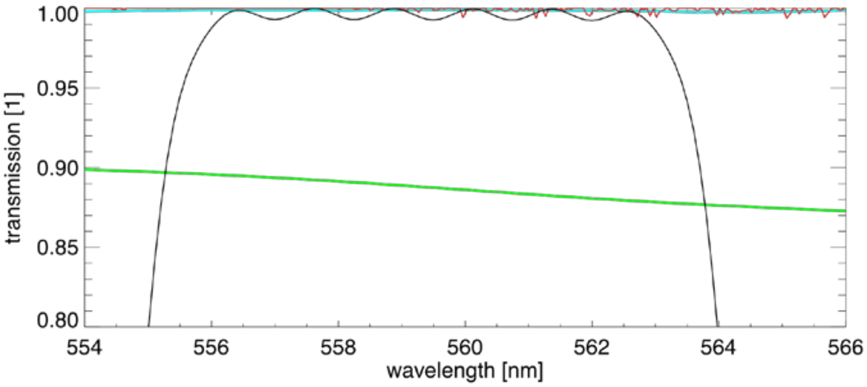

Figure 7: Transmission within channel@560nm, see figure 2

Channel 620 nm - sediment

This channel is affected quite strongly by ozone (figure 8). A correction of the impact of the absorption of ozone is inevitable.

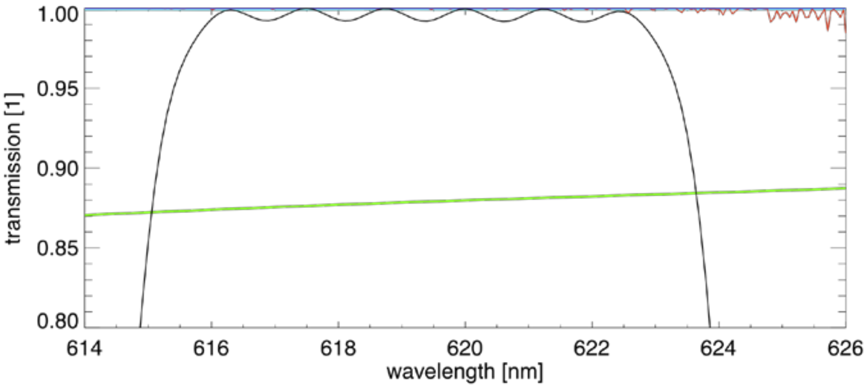

Figure 8: Transmission within channel@620nm, see figure

Channel 665 nm – sediment and chlorophyll fluorescence

This channel is affected quite strongly by ozone (figure 9). Water vapour can contribute to a reduction of the signal by 0.5% (see also table 2). A correction of the impact of the absorption of ozone is inevitable and of water vapour recommended.

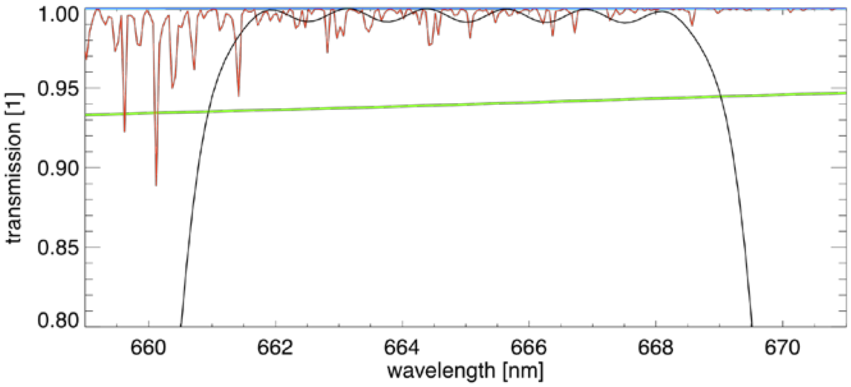

Figure 9: Transmission within channel@665nm, see figure 2

Channel 673.75 nm – sediment and chlorophyll fluorescence

This channel is affected quite strongly by ozone (figure 10). Water vapour does not contribute to a reduction of the signal (see also table 2). A correction of the impact of the absorption of ozone is inevitable.

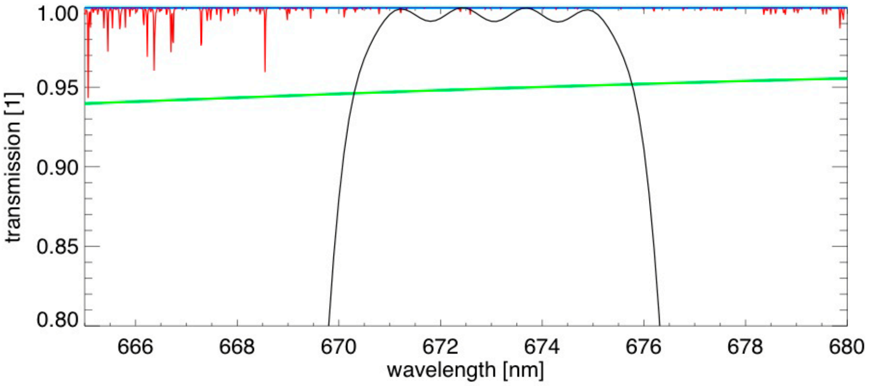

Figure 10: Transmission within channel@673.75nm, see figure 2.

Channel 681.25 nm - chlorophyll fluorescence

This channel is also affected quite strongly by ozone (figure 11). Water vapour reduces the signal by 0.25% in a mid-latitude summer atmosphere (table 2). A correction of the impact of the absorption of ozone is inevitable. The stronger oxygen absorption B-band is roughly 2nm away and will not influence the signal even when a smile shift of ±1nm is considered.

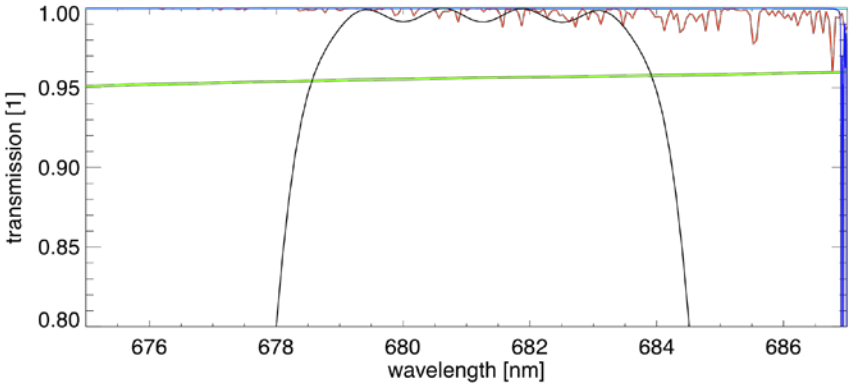

Figure 11: Transmission within channel@681.25nm, see figure 2.

Channel 708 nm – atmospheric correction and chlorophyll fluorescence

This channel is affected quite strongly by water vapour (figure 12). Since the water vapour absorption is quite strong and the lines are not homogenously distributed within the channel, the smile effect contributes also to variations in the measured signal (table 2). When the centre wavelength varies by ±1 nm the transmission changes from 92. 117% (-1nm) to 93.066% (+1nm).

An example is given in figure 12, showing a MERIS RGB and the fluorescence line height off-coast Vancouver Island. Stripes are clearly visible in the fluorescence and MCI images, which might point to an insufficient correction of water vapour absorption and smile effect.

A correction of the impact of water vapour considering the smile effect is necessary as well to perform a reliable atmospheric correction and estimation of the fluorescence signal.

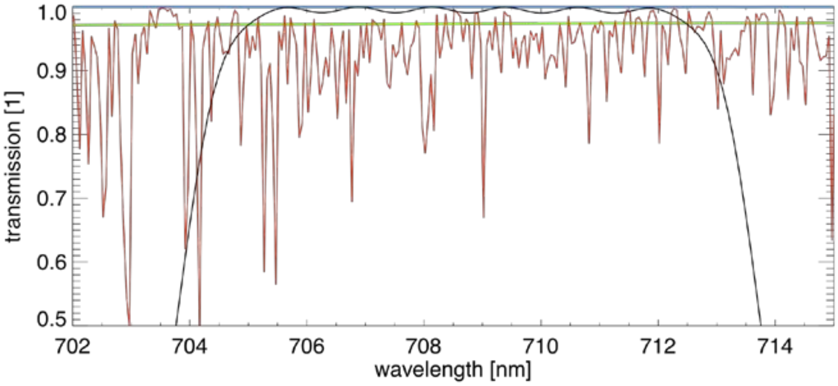

Figure 12: Transmission within channel@708.75nm, see figure 2.

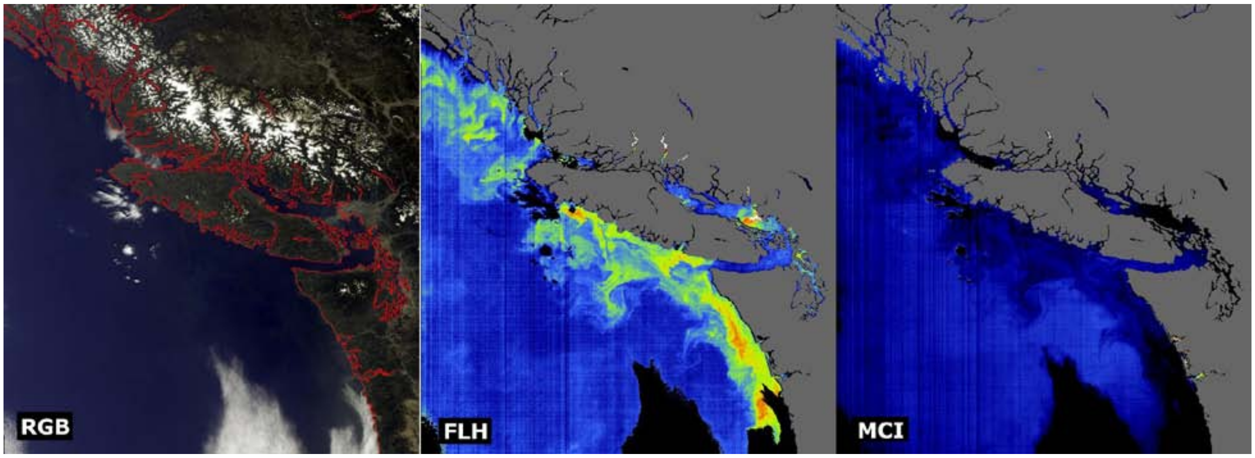

Figure 13: MERIS RGB, fluorescence line height and MCI (priv. com. J. Gower, 2009).

Channel 753.75 nm – cloud and land

This channel is affected mainly by ozone (figure 14). Ozone can reduce the signal by 2% (table 2). A correction of the impact of the absorption of ozone has to be performed.

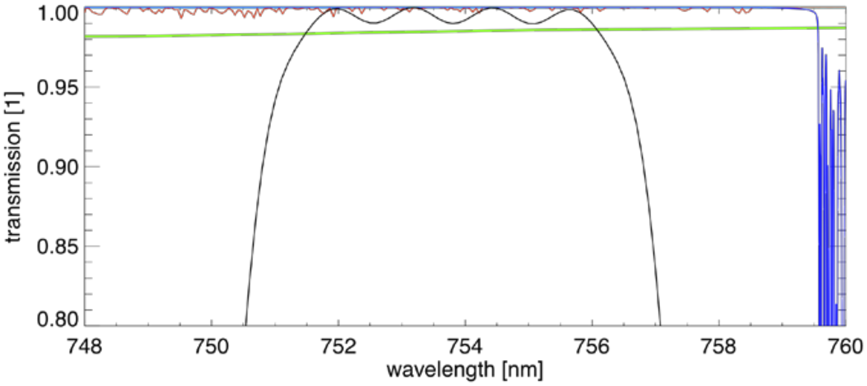

Figure 14: Transmission within channel@753.75nm, see figure 2.

Channels 760.675, 763.75, 768.125 – cloud and land

The OLCI channels within the oxygen A-band are defined to retrieve surface and cloud top pressure. The position and width of the O_2 A-band channels have been redefined by a rigorous information content analysis (Lindstrot et al., 2009). Following the maximal information content and degrees of freedom the channel setting might be composed of a narrow channel in the centre of the R-branch (2 micro-cells at 760 and 761.25nm), a wider channel composed of the next 4 consecutive micro-cells (762.5nm, 763.75nm, 765nm, 766.25nm). The third channel is composed of the next 2 micro-cells (767.5nm, 768.75nm).

Since measurements within the oxygen A-band are used to identify clouds, to retrieve cloud properties or to estimate aerosol scaling heights, which all are subject of specialized algorithms; a correction of the impact of oxygen absorption is not a matter of interest.

However, a correction of the impact of ozone absorption is recommended, since a reduction of the signal of more than 1% appears in the O_2 A-band channels.

Channel 778.75 nm – atmospheric correction

This channel is affected quite strongly by ozone (figure 15). Water vapour can reduce the signal by less than 0.1% in the presence of a mid-latitude summer atmosphere (table 2). A correction of the impact of ozone absorption has to be performed. There is an impact of residual oxygen absorption and also the necessity to consider the smile effect of the cameras, which is described in detail in chapter 2.2.

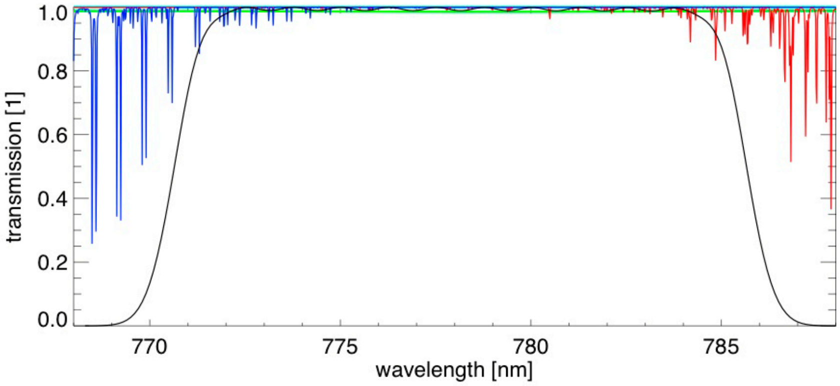

Figure 15: Transmission within channel@778.75nm, see figure 2.

Channel 865.0 nm – aerosols and atmospheric correction

This channel is affected only by water vapour to a minor extent (figure 16). Water vapour can reduce the signal by 0.5% in case of a mid-latitude summer atmosphere (table 2). Even when the impact of water vapour is small, a correction should be applied to reduce the uncertainties.

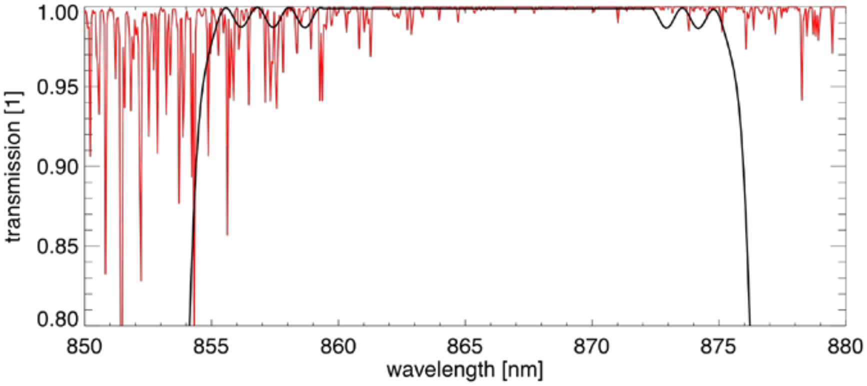

Figure 16: Transmission within channel@865nm, see figure 2.

Channel 885 nm – water vapour reference channel

This channel will mainly used as a reference channel to estimate the water vapour content (figure 17). Nevertheless, this channel is also affected by water vapour reduces the signal by more than 2% in a mid-latitude summer atmosphere (table 2). A correction of the impact of water vapour has to be performed when this channel is used for land or ocean surface applications.

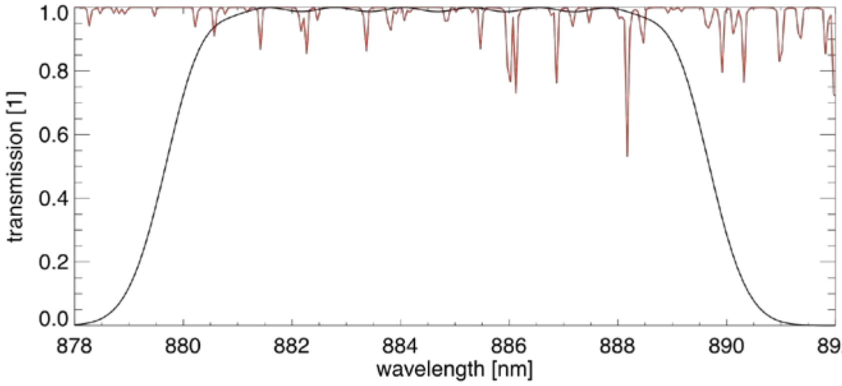

Figure 17: Transmission within channel@885nm, see figure 2.

Channel 900 nm – water vapour

This channel is affected quite strongly by water vapour (figure 18) and used for the retrieval of water vapour columns.

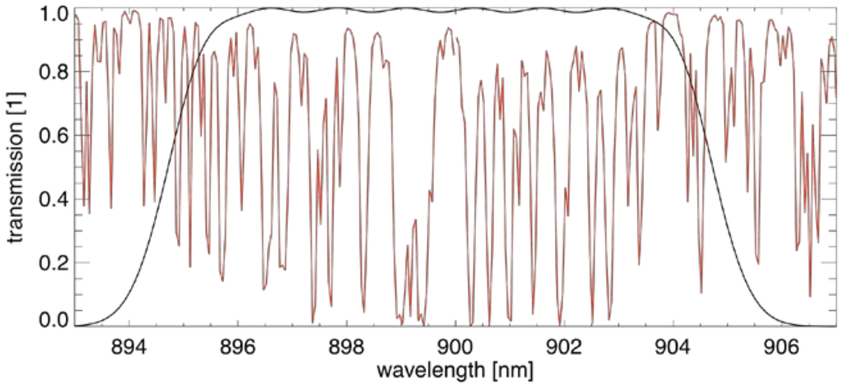

Figure 18: Transmission within channel@900nm, see figure 2.

Channel 940 nm – water vapour

This newly defined OLCI channel is strongly affected by water vapour and used for an improvement of the retrieval of water vapour columns (figure 19).

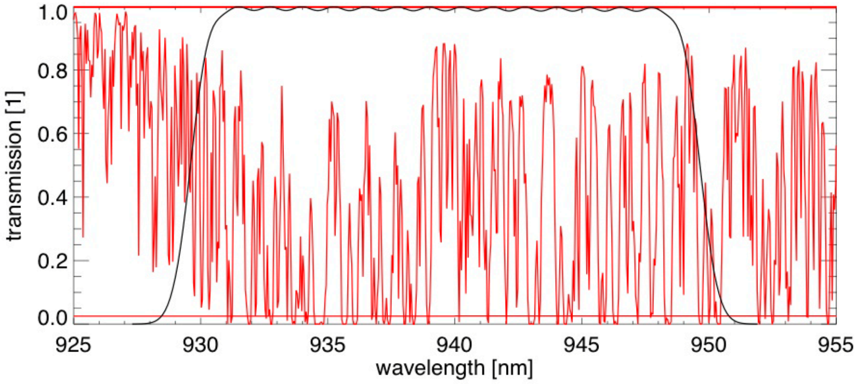

Figure 19: Transmission within channel@940nm, see figure 2.

Channel 1020 nm – water vapour, aerosols and snow

The 1020nm channel is newly defined for the OLCI mission (figure 20). It can be used as the long-wave reference channel to reduce the impact of spectral surface albedo variations in the water vapour retrieval as well as in the retrieval of land surface and snow properties. This channel is mainly affected by water vapour and to a minor extent by carbon dioxide, which reduce the signal by 2% and 0.05% (table 2). A correction of the impact of the absorption of water vapour has to be performed.

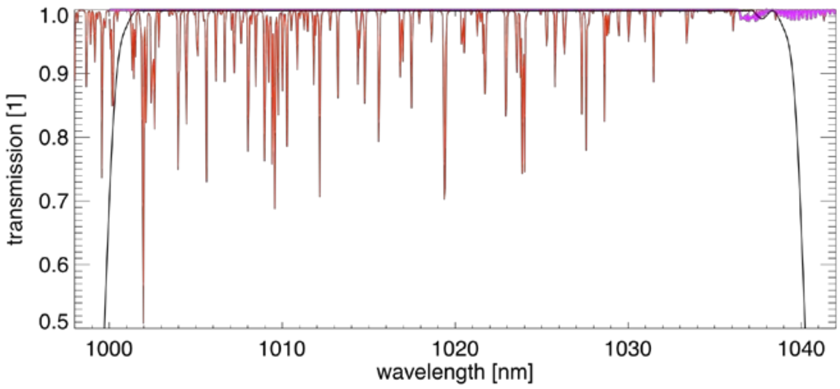

Figure 20: Transmission within channel@1020nm, see figure 2.

Channel	wavelength [nm]	width [nm]	T_H2O	T_O3	T_NO2
O 1	400	15	0.9988	0.9998	0.9879
O 2	412.5	10	0.9998	0.9994	0.9882
O 3	442.5	10	0.9976	0.9956	0.9905
O 4	490	10	0.9991	0.9759	0.9943
O 5	510	10	0.9907	0.9531	0.9958
O 6	560	10	0.9997	0.8860	0.9986
O 7	620	10	0.9999	0.8796	0.9995
O 8	665	10	0.9950	0.9398	0.9999
O 9	673.75	7.5	0.9999	0.9498	0.9999
O 10	681.25	7.5	0.9977	0.9561	0.9999
O 11	708.75	10	0.9262	0.9736	0.9999
	708.75 – 1.	10	0.9212	0.9737	0.9999
	708.75 + 1.	10	0.9307	0.9737	0.9999
O 12	753.75	7.5	0.9991	0.9849	0.9999
O 13	761.25	2.5	1.0	0.9873	0.9999
O 14	764.375	3.75	1.0	0.9876	1.0
O 15	767.5	2.5	1.0	0.9878	1.0
O 16	778.75	15	0.9974	0.9882	1.0
O 17	865	20	0.9957	1.0	1.0
O 18	885	10	0.9798	1.0	1.0
O 19	900	10	0.6830	1.0	1.0
O 20	940	20	0.3339	1.0	1.0
O 21	1020	40	0.9812	1.0	1.0

Table 2: OLCI channel number, central wavelength, spectral width as well as transmission due to water vapour T_H2O, ozone T_O3 and nitrogen dioxide T_NO2; a mid-latitude summer atmosphere and an air-mass factor of 3 is assumed.

2.2 Example - Study on the impact of residual oxygen absorption for the 778 nm MERIS channel

This investigation is performed to understand the impact of even minor absorption processes in the atmosphere and how the measured signals of the MERIS 778nm channel are modified. The MERIS channel at 778nm with a half-width of 15nm has been mainly defined for the retrieval of aerosols and atmospheric correction above ocean. This band is located at the long-wave end of the oxygen A-band. Due to some isolated absorption lines of oxygen, the transmission at 778nm is slightly reduced as compared to a pure window channel. This offset is not constant but depends on the centre wavelength of each individual band 12 (spectral smile effect), the viewing geometry and the brightness of the observed scene.

Figure 21 shows the atmospheric transmission at 778.5nm for an AOT=0.1, depending on the viewing geometry. The transmission varies roughly between 0.9955 and 0.9985. This means that the absorption is indeed very weak but above the MERIS sensor noise level. Therefore, retrieval algorithms based on 778nm data should account for the absorption of oxygen.

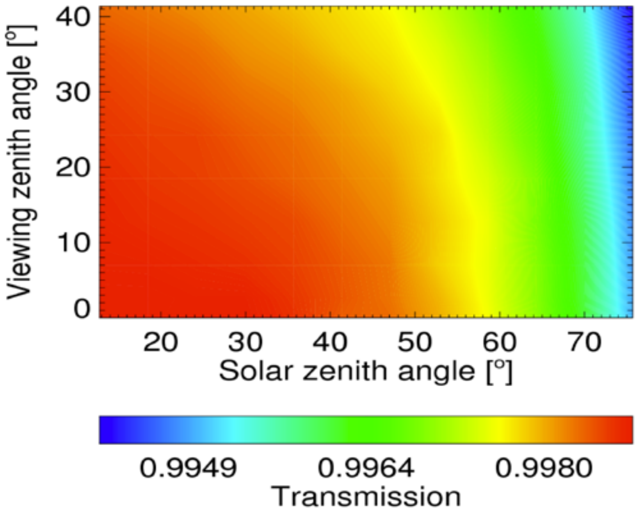

Figure 21: Atmospheric transmission at 778.5nm above ocean for an AOT=0.1, depending on viewing geometry (azimuth angle = 0°).

The spectral variation of the oxygen absorption in the 777.5nm – 779.5nm region are displayed in figure 22 for two selected viewing geometries (view zenith = 0°, solar zenith =30°; viewing zenith=40°, solar zenith =60°). For the shown cases, the amplitude of the variation is 0.13% of transmission for both aerosol loadings. The maximum amplitude of the transmission variations are shown in figure 23 for AOT=0.1 and AOT=0.5 at a scale height of 2km and all combinations of viewing / solar zenith angles. The amplitude is below 0.15% of the transmission for solar zenith angles below 70°. There is hardly any effect of aerosol optical thickness or scale height on the transmission.

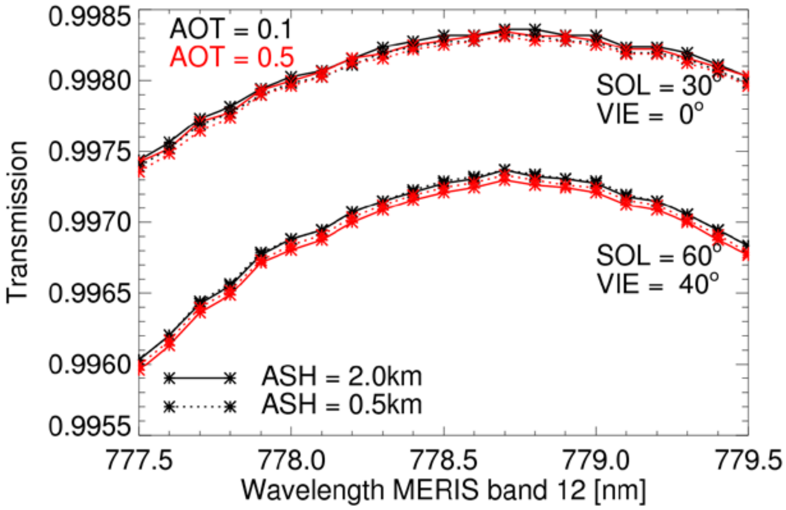

Figure 22: Atmospheric transmission around 778nm for an AOT=0.1 and 0.5 and aerosol scale height of 0.5 and 2km, respectively, depending on centre wavelength of MERIS band 12.

The absorption of oxygen is small (transmission is in the range 0.997±0.0015) but above the MERIS sensor noise level. The spectral variations of the transmission due to the spectral smile of MERIS band 12 are in the range of 0.001 – 0.002 and thus comparable to the variations due to the viewing geometry. The effect of aerosols is negligible.

However, this analysis has been made for MERIS channel 778, whereby the current definition of this channel for OLCI has a centre wavelength at 781.25nm with a reduced channel width of 10nm, which all lead to a reduction of atmospheric absorption processes.

This example illustrates that even weak atmospheric absorption features have to be corrected to achieve the desired accuracy and to avoid striping effects due to the smile of the cameras. A change in the signal along the viewing angle of up 1% above a mid-latitude summer atmosphere is predicted. Following the current definition of the OLCI channels and this investigation, at least channel 708.75nm has to be corrected with respect to the smile effect.

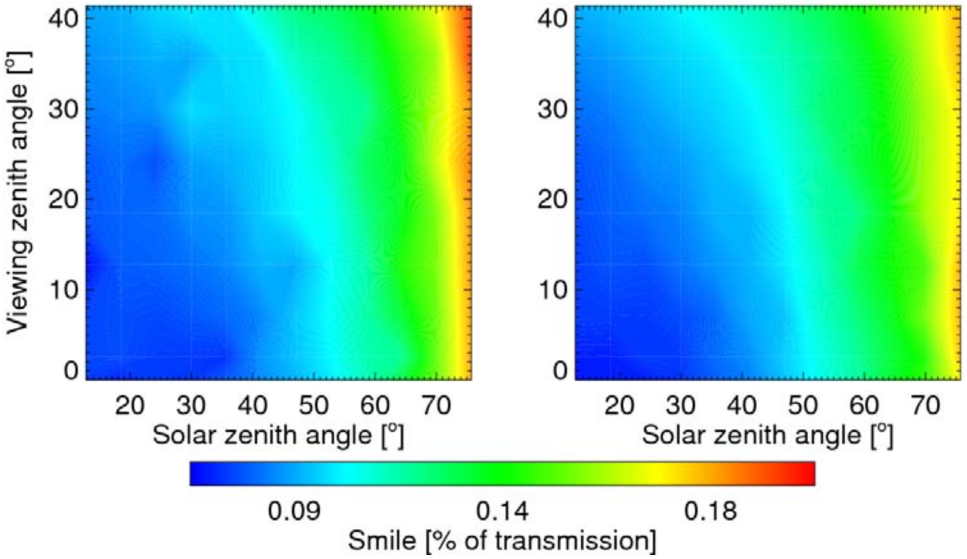

Figure 23: Maximum amplitude of smile effect in MERIS band 12 transmission for AOT=0.1 (left panel) and AOT=0.5 (right panel), depending on viewing geometry (azimuth angle = 0°, ASH=2km).

3. ALGORITHM DESCRIPTION

3.1 Theoretical Description

This part of the ATBD describes the correction of OLCI L1 data with respect to the absorption of atmospheric gases.

To develop a procedure for the correction of the impact of the absorption of atmospheric gases the following steps are recommended:

1. Estimate the transmission functions of all relevant gases and channels
2. Depending on the vertical profile of the absorbing gases a
    a. simple multiplication of the transmission function, or
    b. regression, based on radiative transfer simulations, has to be established
3. Provide the necessary input, such as concentrations of NO_2, O_3 and H_2O, from complementary Sentinel 3 data or other sources.

Radiative transfer simulations are preferred to produce the Look-Up-Tables (LUT) for the correction of atmospheric gases. The Matrix Operator Model MOMO (Fell and Fischer, 2001) is well suited to serve the required database. The gaseous absorption by atmospheric gases is calculated using the line-by-line code XTRA (Rathke and Fischer, 2000), which uses the HITRAN 2008 spectroscopic database (Rothman et al., 2009). From these simulations the transmission functions can be directly estimated. An advanced k-distribution technique (Bennartz and Fischer, 2000) is applied to simulate non line-by-line absorption coefficients, necessary to avoid time-consuming line-by-line complex radiative transfer simulations.

The temperature profile has been assumed to follow so-called standard atmospheres, such as the US and mid-latitude summer, with a surface pressure of 1013hPa. The aerosol optical thickness might be fixed to a value of 0.1, using a maritime aerosol model, in order to consider the competing and non-linear effects of scattering and absorption. Since the transmission usually depends also on the surface reflectivity (i.e. see figure 22), the brightness had to be taken into account somehow. A Lambertian reflector with a variable albedo between 0 and 1 is sufficient to describe the surface impact.

A general procedure for the correction of atmospheric gases should consider:

1. Viewing geometry to estimate the air-mass
2. When the non-isotropic scattering due to aerosols is involved, it is necessary to add three dimensions (_SUN, _V IEW, _DIFF) to the LUT instead of reducing the viewing geometry to air-mass. Especially above dark surfaces, the phase function of the aerosol results in viewing geometry dependence of the transmission.
3. When non-linear scattering and absorption processes modify the signal, the correction procedure should be based on complex radiative transfer simulations.

In the following 2 examples of a correction procedure are described.

1. Ozone correction for the 560nm channel

Generate LUT of transmission functions of ozone between 552nm and 568nm and fold these functions with the filter function of channel 560nm. Since the spectral absorption coefficients of ozone are nearly constant within this spectral range, the smile effect might be not considered. The LUT contain the transmission depending on viewing geometry (air-mass) and ozone concentration. The correction will be applied to the level 1b data, considering the actual ozone concentration.

2. Water vapour correction for the 709nm channel

Generate LUT of transmission functions between 700nm and 715nm by a line-by-line model and estimate from this database the k-coefficients to consider the water vapour absorption in a complex radiative transfer model, such as MOMO. Generate LUT of radiances as a function of viewing geometry, water vapour content, aerosol load and surface reflectivity. Above ocean a rough surface following Cox and Munk (1954) should be used. The LUT should contain an additional dimension to account for the smile effect, thus the radiances should be simulated with different centre wavelength, covering the spectral range of each channel and camera.

The LUT has 5 dimensions, namely the centre wavelength of OLCI band 10, the solar and viewing zenith angles _SUN and _V IEW and the azimuth distance _DIFF, and the water vapour content. Here, the azimuth distance is defined as in MOMO, which is the opposite of MERIS (as an orientation: For _DIFF _ 0o we would expect sun glint).

In order to extract the transmission in band 10 from the LUT, a five-dimensional interpolation among the closest LUT grid-points has to be performed.

3. Recommendation for the correction of atmospheric correction

All OLCI channels have to be corrected to account for the absorption of atmospheric gases. The transmission due to the atmospheric gases, such as water vapour, ozone, and nitrogen dioxide, are listed in table 2.

The channels at 400nm, 412.5nm and 442.5nm have to be corrected for the NO2 absorption. Water vapour should be considered for the 442.5nm channel as well. At least a simple correction applying the corresponding transmission functions should be developed. The provision of actual NO2 concentration might be difficult and could lead to inaccuracies in the correction.

All channels between 490nm and 781.25nm are subject of ozone absorption correction. A simple correction procedure by multiplying the transmission function to the top of radiances might be sufficient.

The channels at 510nm and 665nm are also subject of water vapour absorption. The transmission due to water vapour should be considered with respect to the actual water vapour amount.

Channel 709nm is significantly influenced by water vapour. A necessary correction procedure is described above.

The channels at 885nm and 1020nm are also subject of water vapour absorption. A correction is necessary, whereby a simple correction by transmission functions might be sufficient.

3.2 Practical consideration

The applied correction procedure might be based on LUT, polynomials and neural nets, however, the different approached should be tested against accuracy and applicability.

The impact of the atmospheric gases which have a significant impact within the spectral domains of the OLCI channels are given in Table 2. We propose a simple correction for channels where the absorption is weak or where the absorber mass is mainly in upper atmospheric layers. Channels, which are influenced by stronger water vapour absorption in lower atmospheric layers where multiple scattering effects become relevant as well as where the smile effect can not be neglected, are corrected by a more complex procedure as discussed above (see Chapter 2.2). This is proposed for channel O_11 at 708.75nm and O_16 at 778.75nm and will be discussed below.

The general procedure to correct the measured signal L_{sat} to account for the impact of the absorbing atmospheric gases is a simple division as follows

$$L_{cor} = L_{sat} / T_{gas} \qquad [1]$$

The transmission T_{gas} has to be estimated from the effective absorption coefficient of each atmospheric gas within the spectral domain of an OLCI channel $a_{gas}[\lambda]$, its normalized concentration c^n_{gas} and the air-mass m_{air} which is calculated from the viewing geometry (solar zenith distance and viewing angle).

$$T_{gas}[\lambda] = \exp(-a_{gas}[\lambda]*c^n_{gas}*m_{air})$$

$$c^n_{gas} = c_{gas}/ c^{standard}_{gas} \qquad [2]$$

$$m_{air} = 1/\cos\theta_{sun} + 1/\cos\theta_{view}$$

The table contains the effective absorption coefficient for each gas and each channel. The effective absorption coefficient a_{gas} is defined for a standard absorber mass $c^{standard}_{gas}$, estimated from a line-by-line calculations, applying the actual HITRAN database, and considering the respective channel response function. The actual absorber mass c_{gas} is taken from satellite measurements or climatology. The simple approach is only valid for weak absorption lines, where saturation of individual lines can be neglected.

Consequently, the lookup tables contain for each channel up to three effective absorption coefficients a_{gas} and the standard absorber masses $c^{standard}_{gas}$.

Channel O_1@400nm

Channel O_1 at 400nm has to be corrected for the impact of NO2 with respect to Eq.[1] and Eq.[2]. The apparent transmission T_{gas} is estimated by

$$T_{gas}[O\_1] = \exp(-a_{NO2}[O\_1]*c^n_{NO2}*m_{air})$$

The table contains the absorption coefficient of aNO2 for channel O_1 and the standard absorber mass $c^{standard}_{NO2}$.

Channel O_2@412.5nm

Channel O_2 at 412.5nm has to be corrected for the impact of NO2 with respect to Eq.[1] and Eq.[2]. The apparent transmission T_{gas} is estimated by

$$T_{gas}[O\_2] = \exp(-a_{NO2}[O\_2]*c^n_{NO2}*m_{air})$$

The table contains the absorption coefficient of aNO2 for channel O_2 and the standard absorber mass $c^{standard}_{NO2}$.

Channel O_3@442.5nm

Channel O_3 at 442.5nm has to be corrected for the impact of NO2, O3 and H2O with respect to Eq.[1] and Eq.[2]. The apparent transmission T_{gas} is estimated by

$$\begin{aligned} T_{gas}[O\_3] = {} & \exp(-a_{NO2}[O\_3]*c^n_{NO2}*m_{air}) \\ & * \exp(-a_{H2O}[O\_3]*c^n_{H2O}*m_{air}) \\ & *\exp(-a_{O3}[O\_3]*c^n_{O3}*m_{air}) \end{aligned}$$

The table contains the absorption coefficients a_{NO2}, a_{H2O}, a_{O3} for channel O_3 and the standard absorber masses $c^{standard}_{NO2}$, $c^{standard}_{H2O}$, $c^{standard}_{O3}$.

Channel O_4@490nm

Channel O_4 at 490nm has to be corrected for the impact of NO2 and O3 with respect to Eq.[1] and Eq.[2]. The apparent transmission T_{gas} is estimated by

$$\begin{aligned} T_{gas}[O\_4] = {} & \exp(-a_{NO2}[O\_3]*c^n_{NO2}*m_{air}) \\ & *\exp(-a_{O3}[O\_4]*c^n_{O3}*m_{air}) \end{aligned}$$

The table contains the absorption coefficients a_{NO2}, a_{O3} for channel O_4 and the standard absorber masses $c^{standard}_{NO2}$, $c^{standard}_{O3}$.

Channel O_5@510nm

Channel O_5 at 510nm has to be corrected for the impact of NO2, O3 and H2O with respect to Eq.[1] and Eq.[2]. The apparent transmission T_{gas} is estimated by

$$\begin{aligned} T_{gas}[O\_5] = {} & \exp(-a_{NO2}[O\_5]*c^n_{NO2}*m_{air}) \\ & * \exp(-a_{H2O}[O\_5]*c^n_{H2O}*m_{air}) \\ & *\exp(-a_{O3}[O\_5]*c^n_{O3}*m_{air}) \end{aligned}$$

The table contains the absorption coefficients a_{NO2}, a_{H2O}, a_{O3} for channel O_5 and the standard absorber masses $c^{standard}_{NO2}$, $c^{standard}_{H2O}$, $c^{standard}_{O3}$.

Channel O_6@560nm

Channel O_6 at 560nm has to be corrected for the impact of NO2 and O3 with respect to Eq.[1] and Eq.[2]. The apparent transmission T_{gas} is estimated by

$$T_{gas}[O\_6] = \exp(-a_{NO2}[O\_6]*c^n{}_{NO2}*m_{air})$$
$$*\exp(-a_{O3}[O\_6]*c^n{}_{O3}*m_{air})$$

The table contains the absorption coefficients a_{NO2}, a_{O3} for channel O_6 and the standard absorber masses $c^{standard}{}_{NO2}$, $c^{standard}{}_{O3}$.

Channel O_7@620nm

Channel O_7 at 620nm has to be corrected for the impact of H2O with respect to Eq.[1] and Eq.[2]. The apparent transmission T_{gas} is estimated by

$$T_{gas}[O\_7] = \exp(-a_{H2O}[O\_7]*c^n{}_{H2O}*m_{air})$$

The table contains the absorption coefficient a_{H2O} for channel O_7 and the standard absorber mass $c^{standard}{}_{H2O}$.

Channel O_8@665nm

Channel O_8 at 665nm has to be corrected for the impact of O3 and H2O with respect to Eq.[1] and Eq.[2]. The apparent transmission T_{gas} is estimated by

$$T_{gas}[O\_8] = \exp(-a_{H2O}[O\_8]*c^n{}_{H2O}*m_{air})$$
$$*\exp(-a_{O3}[O\_8]*c^n{}_{O3}*m_{air})$$

The table contains the absorption coefficients a_{H2O}, a_{O3} for channel O_8 and the standard absorber masses $c^{standard}{}_{H2O}$, $c^{standard}{}_{O3}$.

Channel O_9@673.75nm

Channel O_9 at 673.75nm has to be corrected for the impact of O3 and H2O with respect to Eq.[1] and Eq.[2]. The apparent transmission T_{gas} is estimated by

$$T_{gas}[O\_9] = \exp(-a_{H2O}[O\_9]*c^n{}_{H2O}*m_{air})$$
$$*\exp(-a_{O3}[O\_9]*c^n{}_{O3}*m_{air})$$

The table contains the absorption coefficients a_{H2O}, a_{O3} for channel O_9 and the standard absorber masses $c^{standard}{}_{H2O}$, $c^{standard}{}_{O3}$.

Channel O_10@681.25nm

Channel O_9 at 681.25nm has to be corrected for the impact of O3 and H2O with respect to Eq.[1] and Eq.[2]. The apparent transmission T_{gas} is estimated by

$$T_{gas}[O\_9] = \exp(-a_{H2O}[O\_9]*c^n{}_{H2O}*m_{air})$$
$$*\exp(-a_{O3}[O\_9]*c^n{}_{O3}*m_{air})$$

The table contains the absorption coefficients a_{H2O}, a_{O3} for channel O_10 and the standard absorber masses $c^{standard}_{H2O}$, $c^{standard}_{O3}$.

Channel O_11@708.75nm

Channel O_11 at 708.75nm has to be corrected for the impact of O3 and H2O. The apparent transmission T_{gas} is estimated by

$$T_{gas}[O\_11] = \exp(-a_{O3}[O\_11] * con_{O3} * m_{air}) \quad * \quad T_{H2O}(a_{H2O}, \tau_a, L^n_{TOA}, \theta_{view}, \theta_{sun}, \phi_{diff}, \lambda)$$

The impact of O3 is corrected using absorption coefficient of a_{O3} for channel O_11 and the standard absorber mass $c^{standard}_{O3}$.

The correction for H2O is more complex, since the absorption within channel O_11 is quite strong with saturating effects of individual lines and due to multiple scattering effects. Furthermore, H2O absorption lines are not spectrally homogeneously distributed within channel O_11 and thus the smile effect becomes more important. In contrast to the previous approaches, the apparent transmission T_{H2O} will directly be calculated form a look up table. The calculation will be a linear interpolation in the following dimensions:

1. absorber mass of H2O a_{H2O},
2. aerosol optical thickness τ_a,
3. normalized L^n_{TOA} radiance in channel 11
4. viewing zenith θ_{view}
5. sun zenith θ_{sun}
6. viewing azimuth ϕ
7. and actual central wavelength λ

The 7 dimension of this look-up table will have presumably 10 nodes for a_{H2O}, 5 nodes for τ_a, 9 nodes for $\mathbf{L^n_{TOA}}$, 8 values for the zenith angles, 7 angles for the azimuth, 10 values for λ_{O_11}, leading to a size of approximately 7 MB. (The actually number of nodes per dimension shall be implemented flexible, since they may a subject of future change).

The look up table will be filled using sophisticated radiative transfer simulations.

Channel O_12@753.75nm

Channel O_11 at 753.75nm has to be corrected for the impact of O3 and H2O with respect to Eq.[1] and Eq.[2]. The apparent transmission T_{gas} is estimated by

$$T_{gas}[O\_12] = \exp(-a_{O3}[O\_12]*c^{n}_{O3}*m_{air})$$

The table contains the absorption coefficients a_{O3} for channel O_12 and the standard absorber mass $c^{standard}_{O3}$.

Channel O_13@761.25nm

Channel O_13 at 761.25nm has to be corrected for the impact of O3 and H2O with respect to Eq.[1] and Eq.[2]. The apparent transmission T_{gas} is estimated by

$$T_{gas}[O\_13] = \exp(-a_{O3}[O\_13]*c^{n}_{O3}*m_{air})$$

The table contains the absorption coefficients a_{O3} for channel O_13 and the standard absorber mass $c^{standard}_{O3}$.

Channel O_14@764.375nm

Channel O_14 at 764.375nm has to be corrected for the impact of O3 with respect to Eq.[1] and Eq.[2]. The apparent transmission T_{gas} is estimated by

$$T_{gas}[O\_14] = \exp(-a_{O3}[O\_14]*c^{n}_{O3}*m_{air})$$

The table contains the absorption coefficients a_{O3} for channel O_14 and the standard absorber mass $c^{standard}_{O3}$.

Channel O_15@767.5nm

Channel O_15 at 767.5nm has to be corrected for the impact of O3 with respect to Eq.[1] and Eq.[2]. The apparent transmission T_{gas} is estimated by

$$T_{gas}[O\_15] = \exp(-a_{O3}[O\_15]*c^{n}_{O3}*m_{air})$$

The table contains the absorption coefficients a_{O3} for channel O_15 and the standard absorber mass $c^{standard}_{O3}$.

Channel O_16@778.75nm

Channel O_16 at 778.75nm has to be corrected for the impact of O3 and H2O. The apparent transmission T_{gas} is estimated by

$$T_{gas}[O\_16] = \exp(-a_{O3}[O\_16]*con_{O3}*m_{air}) \quad * \quad T_{O2}(a_{O2}, \tau_a, L^{n}_{TOA}, \theta_{view}, \theta_{sun}, \phi_{diff}, \lambda)$$

The impact of O3 is corrected using absorption coefficient of a_{O3} for channel O_16 and the standard absorber mass $c^{standard}_{O3}$.

The correction for O2 is more complex, since the absorption lines are not spectrally homogeneously distributed within channel O_16 and thus the smile effect becomes more important. In contrast to the previous approaches, the apparent transmission T_{O2} will directly be calculated from a look up table. The calculation will be a linear interpolation in the following dimensions:

1. absorber mass of O2 $a_{O2,}$
2. aerosol optical thickness τ_a,
3. normalized L^n_{TOA} radiance in channel 16
4. viewing zenith θ_{view}
5. sun zenith θ_{sun}
6. viewing azimuth ϕ
7. and actual central wavelength λ

The 7 dimension of this look-up table will have presumably 10 nodes for a_{O2}, 5 nodes for τ_a, 9 nodes for L^n_{TOA}, 8 values for the zenith angles, 7 angles for the azimuth, 10 values for λ_{O_11}, leading to a size of approximately 7 MB. (The actually number of nodes per dimension shall be implemented flexible, since they may a subject of future change).

The look up table will be filled using sophisticated radiative transfer simulations.

Channel O_17@865nm

Channel O_17 at 865nm has to be corrected for the impact of H2O with respect to Eq.[1] and Eq.[2]. The apparent transmission T_{gas} is estimated by

$$T_{gas}[O\_17] = \exp(-a_{H2O}[O\_17]*c^n_{H2O}*m_{air})$$

The table contains the absorption coefficients a_{H2O} for channel O_17 and the standard absorber mass $c^{standard}{}_{H2O}$.

Channel O_18@885nm

Channel O_18 at 885nm has to be corrected for the impact of H2O with respect to Eq.[1] and Eq.[2]. The apparent transmission T_{gas} is estimated by

$$T_{gas}[O\_18] = \exp(-a_{H2O}[O\_18]*c^{n}{}_{H2O}*m_{air})$$

The table contains the absorption coefficients a_{H2O} for channel O_18 and the standard absorber mass $c^{standard}{}_{H2O}$.

Channel O_19@900nm

Channel O_19 at 900nm has to be corrected for the impact of O3 and H2O with respect to Eq.[1] and Eq.[2]. The apparent transmission T_{gas} is estimated by

$$T_{gas}[O\_19] = \exp(-a_{H2O}[O\_19]*c^{n}{}_{H2O}*m_{air})$$

The table contains the absorption coefficients a_{H2O} for channel O_19 and the standard absorber mass $c^{standard}{}_{H2O}$.

Channel O_20@940nm

Channel O_20 at 940nm has to be corrected for the impact of H2O with respect to Eq.[1] and Eq.[2]. The apparent transmission T_{gas} is estimated by

$$T_{gas}[O\_20] = \exp(-a_{H2O}[O\_20]*c^{n}{}_{H2O}*m_{air})$$

The table contains the absorption coefficients a_{H2O} for channel O_20 and the standard absorber mass $c^{standard}{}_{H2O}$.

Channel O_21@1020nm

Channel O_21 at 1020nm has to be corrected for the impact of H2O with respect to Eq.[1] and Eq.[2]. The apparent transmission T_{gas} is estimated by

$$T_{gas}[O\_21] = \exp(-a_{H2O}[O\_21]*c^{n}{}_{H2O}*m_{air})$$

The table contains the absorption coefficients a_{H2O} for channel O_21 and the standard absorber mass $c^{standard}_{H2O}$.

4. ASSUMPTIONS AND LIMITATIONS

The accuracy of the correction of atmospheric gases depends on the available nitrogen, ozone and water vapour concentration. Since OLCI has dedicated channels to measure water vapour the latter might be corrected well. The provide HITRAN 2008 database is of high quality.

5. REFERENCES

Albert, P., R. Bennartz, R. Preusker, R. Leinweber und J. Fischer, 2005: Remote Sensing of Atmospheric Water Vapour Using the Moderate Resolution Imaging Spectrometer. J. Atmos. Oceanic Technol., 22, 309-314.

Bennartz, R. and J. Fischer, 2000: A modified k-distribution approach applied to narrow band water vapour and oxygen absorption estimates in the near infrared. J. Quant. Spectrosc. Radiat. Transfer , 66, 539_553.

Boesche, E., P. Stammes, R. Preusker, R. Bennartz, W. Knap, and J. Fischer, 2008: Polarization of skylight in the O2A band: effects of aerosol properties. Appl. Opt. 47, 3467-3480.

Bourg, L., 2010. Instrument Corr ATBD

Delwart, S., R. Preusker, L. Bourg, R. Santer, D. Ramon, and J. Fischer, 2007: MERIS inflight spectral calibration. Int. J. Rem. Sens., 28, 479 – 496.

Fell, F. and J. Fischer, 2001: Numerical simulation of the light field in the atmosphere-ocean system using the matrix-operator method. J. Quant. Spectrosc. Radiat. Transfer , 3, 351_388.

Lindstrot, R., Preusker, R., Ruhtz, T., Heese, B., Wiegner, M., Lindemann, C. and Fischer, J., 2006: Validation of MERIS cloud top pressure using airborne lidar measurements. J. Appl. Meteor. Clim., 45 (12), 1612-1621.

Lindstrot, R., R. Preusker, and J. Fischer, 2009: The retrieval of land surface pressure from MERIS measurements in the oxygen a band. Journal of Atmospheric and Oceanic Technology, 26, 1367 – 1377.

McClatchey, R., R. Fenn, J. Selby, F. Volz, and J. Garing, 1972: Optical Properties of the Atmosphere. Air Force Cambridge Research Laboratories, 3rd edition.

Merheim-Kealy, P., J. P. Huot, and S. Delwart, 1999: The MERIS ground segment.
Int. J. Rem. Sens., 20, 1703–1712.

Preusker, R. and R. Lindstrot, in press: Remote sensing of cloud-top pressure using moderately resolved measurements within the oxygen A band - a sensitivity study. J. Appl. Meteor. Clim., accepted.

Preusker, R., J. Fischer, P. Albert, R. Bennartz, and L. Schüller, 2007: Cloud-top pressure retrieval using oxygen A-band channels of the IRS-3 MOS instrument. Int. J. Remote Sensing, 28, 1957-1967.
Rathke, C. and J. Fischer, 2000: Retrieval of cloud microphysical properties from thermal infrared observations by a fast iterative radiance fitting method, J. Atmos. Oceanic Technol., 17, 1509-1524.

Rast, M., J. L. Bezy, and S. Bruzzi, 1999: The ESA Medium Resolution Imaging Spectrometer MERIS - A review of the instrument and its mission. Int. J. Rem. Sens., 20, 1681–1702.

Rothman, L.S., I.E.Gordon, A. Barbe, D. ChrisBenner, P.F.Bernath, M.Birk, V.Boudon, L.R. Brown, A.Campargue, J.-P.Champion, K.Chance, L.H.Coudert, V.Dana, V.M.Devi, S. Fally,1, J.-M.Flaud, R.R.Gamache, A.Goldmanm, D.Jacquemart, I.Kleiner, N. Lacome, W.J.Lafferty, J.-Y.Mandin, S.T.Massie, S.N.Mikhailenko, C.E.Miller, N. Moazzen-Ahmadi, O.V.Naumenko, A.V.Nikitin, J.Orphal, V.I.Perevalov, A.Perrin, A.Predoi-Cross, C.P.Rinsland, M.Rotger, M.Simeckova, M.A.H.Smith, K.Sung, S.A.Tashkun, J.Tennyson, R.A.Toth, A.C.Vandaele, J.VanderAuwera, 2009: The HITRAN 2008 molecular spectroscopic database. Journal of Quantitative Spectroscopy and Radiative Transfer (*JQSRT*), 110, 533-572.

Santer, R., F. Zagolski, D. Ramon, J. Fischer and P. Dubuisson, 2005: Uncertainties in radiative transfer computations: consequences on the MERIS products over land. Int. J. Remote Sensing, 26, No. 20, 4597–4626.

Schroeder, Th., I. Behnert, M. Schaale, J. Fischer and R. Doerffer, 2007: Atmospheric correction algorithm for MERIS above Case-2 waters. Int. J. Remote Sens., 28, No. 7, 1469-1486

Zieger, P., T. Ruhtz, R. Preusker, and J. Fischer, 2007: Dual-aureole and sun spectrometer system for airborne measurements of aerosol optical properties. Appl. Opt. 46, 8542-8552.